Geotextiles and Geomembranes 43 (2015) 372–381

Contents lists available at ScienceDirect

Geotextiles and Geomembranes

journal homepage: www.elsevier.com/locate/geotexmem

Experimental and numerical studies on protection of buried pipelines and underground utilities using geocells

A.M. Hegde*, T.G. Sitharam

Department of Civil Engineering, Indian Institute of Science, Bangalore, 560012, India

ARTICLE INFO

Article history:
Received 8 October 2014
Received in revised form
21 February 2015
Accepted 25 April 2015
Available online 27 May 2015

Keywords:
Geosynthetics
Buried pipeline
Geocell
Geogrid
Pavement
Bearing pressure

ABSTRACT

This paper presents the results of the laboratory model tests and the numerical studies conducted on small diameter PVC pipes, buried in geocell reinforced sand beds. The aim of the study was to evaluate the suitability of the geocell reinforcement in protecting the underground utilities and buried pipelines. In addition to geocells, the efficacy of only geogrid and geocell with additional basal geogrid cases were also studied. A PVC (Poly Vinyl Chloride) pipe with external diameter 75 mm and thickness 1.4 mm was used in the experiments. The vehicle tire contact pressure was simulated by applying the pressure on the top of the bed with the help of a steel plate. Results suggest that the use of geocells with additional basal geogrid considerably reduces the deformation of the pipe as compared to other types of reinforcements. Further, the depth of placement of pipe was also varied between 1*B* to 2*B* (*B* is the width of loading plate) below the plate in the presence of geocell with additional basal geogrid. More than 50% reduction in the pressure and more than 40% reduction in the strain values were observed in the presence of reinforcements at different depths as compared to the unreinforced beds. Conversely, the performance of the subgrade soil was also found to be marginally influenced by the position of the pipe, even in the presence of the relatively stiff reinforcement system. Further, experimental results were validated with 3-dimensional numerical studies using FLAC^{3D} (Fast Lagrangian Analysis of Continua in 3D). A good agreement in the measured pipe stain values were observed between the experimental and numerical studies. Numerical studies revealed that the geocells distribute the stresses in the lateral direction and thus reduce the pressure on the pipe. In addition, the results of the 1-g model tests were scaled up to the prototype case of the shallow buried pipeline below the pavement using the appropriate scaling laws.

1. Introduction

Underground conduits or utility pipelines form a complex network in the urban areas and are often laid below the pavements and the temporary structures. Often, these conduits or pipelines are buried at shallow depths in trenches with the help of flowable fills. These pipes tend to deform and damage due to application of repeated traffic loads or heavy static loads from the vehicles. The damage leads to the discomfort of the consumers of the utility and also to the travelers on the road. In this research, it is proposed to design a shallow reinforcement system using geocells to bridge these utility lines. Many researchers in the past have studied the design and installation aspects of the buried pipes through small and large scale tests (Brachman et al., 2000; Mir Mohammad Hosseini and Moghaddas Tafreshi, 2002; Arockiasamy et al., 2006; Srivastava et al., 2012).

Nowadays, reinforcing the soil in the form of geosynthetic reinforcement is gaining popularity in geotechnical engineering. These reinforcements increase the overall performance of the foundation bed by increasing the load carrying capacity and reducing the settlement. Many researchers have studied the beneficial effect of the geosynthetic reinforcements in various geotechnical applications (Indraratna et al., 2010; Rowe and Taechakumthorn, 2011; Demir et al., 2013; Bai et al., 2013; Almeida et al., 2014 etc.). However, the use of geosynthetic reinforcement to protect buried pipes and underground utilities is relatively a new concept. Moghaddas Tafreshi and Khalaj (2008) conducted the laboratory studies on small diameter HDPE pipes buried in the geogrid reinforced sand subjected to repeated load. Researchers observed the significant reduction in the deformation of the pipe in the presence of geogrids. Palmeira and Andrade

* Corresponding author. Tel.: +91 8277381341; fax: + 91 80 23600404.
E-mail addresses: amarnathhegde@gmail.com (A.M. Hegde), sitharam@civil.iisc.ernet.in (T.G. Sitharam).

http://dx.doi.org/10.1016/j.geotexmem.2015.04.010
0266-1144/

(2010) used the combination of geotextile and geogrid to protect the buried pipelines in their model studies. Researchers observed that the reinforcement offers significant resistance to sharp, penetrating object and helps to protect the buried pipes from the accidental damages.

In recent times, geocells are showing its efficacy in geotechnical engineering applications. Geocells are 3-dimensional expandable panels made up of ultrasonically welded high strength polymers or the polymeric alloy such as Polyethylene, Polyolefin etc. The interconnected cells in the geocell form a slab that behaves like a large pad that spreads the applied load over a wider area. Many researchers in the past have highlighted the advantages of using the geocells in geotechnical engineering applications (Moghaddas Tafreshi and Dawson, 2010; Pokharel et al., 2010; Lambert et al., 2011; Yang et al., 2012; Thakur et al., 2012; Sitharam and Hegde, 2013; Mehdipour et al., 2013; Hegde and Sitharam, 2014a, b; Moghaddas Tafreshi et al., 2014; Hegde et al., 2014; Indraratna et al., 2014). Tavakoli et al. (2013) highlighted the beneficial use of geocells in protecting the buried pipelines in their studies. Researchers emphasized the importance of selection of the suitable compaction technique to compact the backfill soil above and below the geocells. Tavakoli et al. (2012) used the combination of geocell reinforcement and rubber soil mixture to protect buried pipes. It was observed that the combination of geocell reinforcement and 5% rubber mixed soil (irrespective of the size or type of the rubber) provides the best performance in terms of reduction in the pipe deformation and backfill settlement.

In this paper, a rather simple technique was used. Contrary to the previous studies, the combination of geocell and geogrid was used to protect the underground utilities and buried pipelines. The first part of the manuscript deals with the 1-g model plate load tests while the second part of the manuscript demonstrates the 3-dimensional numerical modeling of the problem.

2. Laboratory tests

2.1. Experimental setup

The experiments were conducted in the test tank of size 900 mm in length, 900 mm in width and 600 mm in height, made up of cast iron. The tank was fitted to the loading frame which was connected to manually operated hydraulic jack. The vehicle tire contact pressure was simulated by applying the pressure on the top of the bed with the help of a steel plate. A square shaped steel plate with 20 mm thickness and 150 mm sides was used for the purpose. The load was applied through a hand operated hydraulic jack. A pre-calibrated proving ring was used to measure the imposed load. To avoid the eccentric application of the load, the ball bearing arrangement was used. Two dial gauges (D_1 and D_2) were placed on the either side of the centerline of the steel plate to record the settlement of the plate. Another set of dial gauges (S_1 and S_2) was placed at the distance of 1.5B (B is the width of the steel plate) from the centerline of the plate to measure the deformation underwent by the fill surface. Schematic representation of test setup is shown in Fig. 1.

2.2. Materials used

Sand used in the investigation was dry sand with specific gravity 2.64, effective particle size (D_{10}) 0.26 mm, coefficient of uniformity (C_u) 3.08, coefficient of curvature (C_c) 1.05, maximum void ratio (e_{max}) 0.81 and minimum void ratio (e_{min}) of 0.51. According Unified Soil Classification System (USCS) the sand was classified as poorly graded sand with symbol SP. Fig. 2 represents the grain size distribution of sand. The geocell used in the study was made of Neoloy.

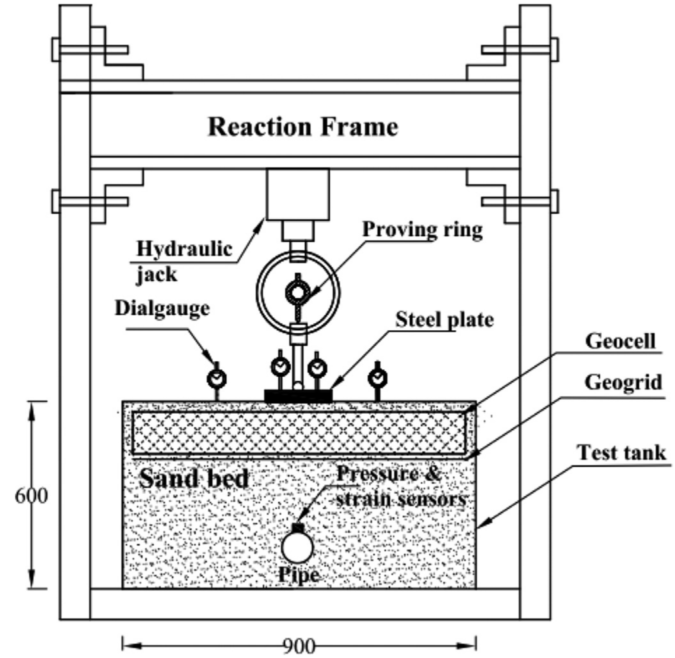

Fig. 1. Schematic view of the test setup.

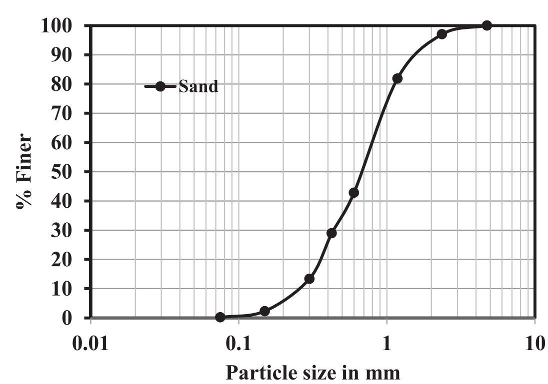

Fig. 2. Grain size distribution curve of sand.

Biaxial geogrid made up of Polypropylene with aperture size 35 mm × 35 mm was used. The properties of the geocell and the geogrid are summarized in Table 1. Pipe used in the study was made up of PVC (Polyvinyl Chloride) with external diameter 75 mm and

Table 1
Properties of the geocell and geogrid.

Parameters	Quantity
Geocell	
Material	Neoloy
Cell size (mm)	250 × 210
No. of cells/m^2	40
Cell depth (mm)	150
Strip thickness (mm)	1.53
Cell seam strength (N)	2150(±5%)
Density (g/cm^3)	0.95 (±1.5%)
Short term yield strength (kN/m)	20
Geogrid	
Polymer	Polypropylene
Aperture size (mm)	35 × 35
Ultimate tensile strength, (same in MD and XMD (kN/m))	20
Mass per unit area (g/m^2)	220
Shape of aperture opening	Square

MD-Machine direction; XMD-Cross machine direction.

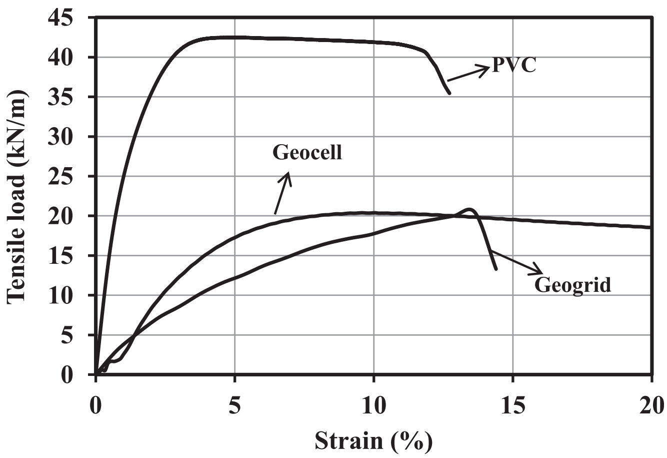

Fig. 3. Tensile load-strain behavior for different materials.

thickness 1.4 mm. The tensile test was conducted on the pipe sample as per the guidelines of ASTM-D638 (2010). From the tensile stress-strain response, the secant modulus of the pipe material corresponding to 2% axial strain was determined as 3.1 GPa. The ultimate tensile strength of the pipe was 42 kN/m. The tensile strength of the geocell strip and the geogrid were determined as per the guidelines of ASTM-D4885 (2011) and ASTM-D6637 (2011) respectively. Tensile load-strain behavior of geocell, geogrid, and pipe material are shown in Fig. 3.

2.3. Preparation of the test bed

First, the sides of the tank were coated with Polythene sheets to avoid the side friction. Pluviation technique was used to prepare the sand bed of 600 mm thick. Before the start of the actual test, a series of trials were conducted to determine the height of fall required to achieve the desired relative density. In each trail, small aluminum cups with known volume were placed at the different locations of the tank. A calibration chart was prepared by knowing the maximum and minimum void ratios of the sand. All the tests were conducted at the constant relative density of 65%. The height of fall required to achieve 65% relative density was directly obtained from the chart. The pipe and the reinforcements were placed at the predetermined depth during the preparation of the sand bed. Geocell pockets were filled up with the sand using the pluviation technique. Fig. 4a–b represents photographs showing the different stages of the bed preparation. After achieving the desired height of the bed, the fill was leveled using a trowel without disturbing the density of the bed.

Table 2
Test details.

Test series	Details	
A	Variable parameters	Type of reinforcement: Unreinforced, only geogrid, only geocell, geocell with basal geogrid
	Constant parameters	$H/B = 1.5$, $b/B = 5.8$,$D/B = 0.5$, $ID = 65\%$
B	Variable parameters	Unreinforced condition $H/B = 1, 1.25, 1.5, 1.75, 2$
	Constant parameters	$D/B = 0.5$, $ID = 65\%$
C	Variable parameters	Geocell with basal geogrid reinforced $H/B = 1, 1.25, 1.5, 1.75, 2$
	Constant parameters	$D/B = 0.5$, $ID = 65\%$,$b/B = 5.8$,$h/B = 1$

2.4. Instrumentation

Strain gauges were mounted on the top surface of the pipe with a half bridge circuit arrangement. Commercial adhesive was used to fix the strain gauges. At each gauge location, the pipe surface was rubbed with a sand paper, before it wiped clean. Strain gauges had normal resistance of 120 Ω and maximum measuring capacity up to 1.5% strain (15,000 micro strains). Just above the strain gauges, exactly at the same locations, three earth pressure cells were placed in the sand bed to measure the vertical stress. Diameter and thickness of the pressure cells were 25 mm and 10 mm respectively. These cells could measure the pressure in the range of 0–10 kg/cm^2 with a least count of 0.1 kg/cm^2. The strain gauges and pressure cells were connected to two separate display units through lead wires.

2.5. Testing program

Three series of plate load tests were conducted. In the first series (A), the tests were conducted with 3 different types of reinforcements with fixed depth of placement of pipe i.e. 1.5B below the steel plate. In the second series, the depth of the pipe was varied between 1B–2B below the plate in the unreinforced condition. In the third series (C), the depth of the pipe was varied between 1B–2B below the steel plate in the presence of geocell with additional basal geogrid. The details of the testing program are summarized in Table 2. The geocell mattress used was square in shape. The diameter of the pipe, size of plate, relative density of the sand bed and the geocell geometry i.e. height, width and pocket size were kept constant in all the tests. The steel plate was placed on the

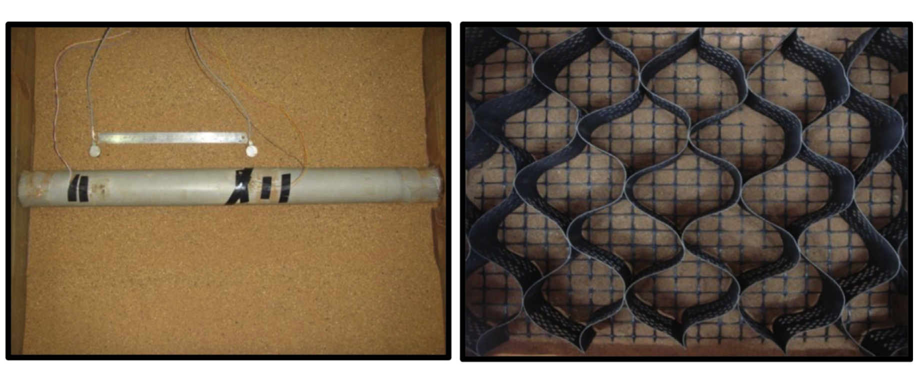

(a) (b)

Fig. 4. Photograph of the test: (a) placement of pipe; (b) expanded geocell

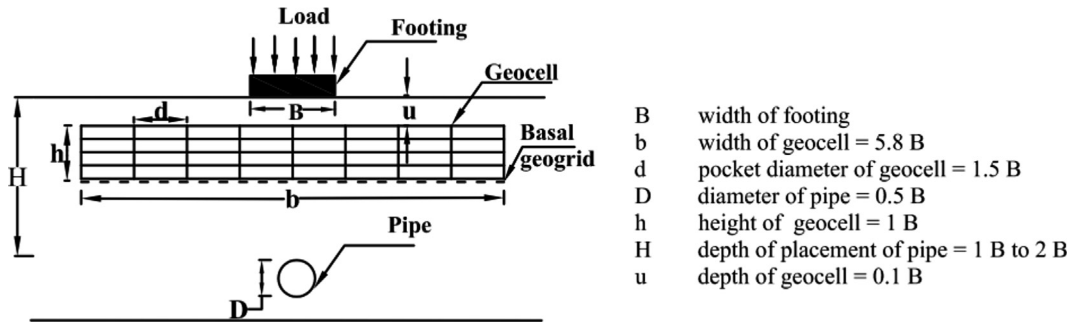

Fig. 5. Geometry of the test configuration.

surface of the sand bed. In reinforced tests, the geocell and geogrid reinforcements were placed to the full width of the tank leaving the small gap between the tank wall and the reinforcement to avert the boundary effects. In other words, the width of the reinforcement was about 5.8 times the width of the steel plate in all the tests. Dash et al. (2001) reported the optimum depth of geocell placement as 0.1B from the bottom of the footing. Hence, in the present investigation, the geocell was placed at the depth of 0.1B below the steel plate. Fig. 5 represents the geometry of the test configuration.

3. Results and discussions

3.1. Effect of reinforcement types

The efficacy of geogrid, geocell and geocell with additional basal geogrid reinforcements in protecting the buried pipelines are compared in this section. Throughout this test series, the pipe was placed at a depth of 1.5B below the loading plate. Fig. 6 represents the bearing pressure-settlement response of the sand bed for the different test cases. For convenience, the settlement (S) of the loading plate was normalized with its width (B). Bearing capacity failure of the sand bed was observed in both unreinforced and geogrid reinforced cases at $S/B = 20\%$ and $S/B = 35\%$ respectively. The failure of the bed was indicated by the sudden reduction in the slope of the pressure-settlement curve i.e. the curve becomes almost vertical. However, no failure was occurred in geocell reinforced case and geocell with additional basal geogrid reinforced case even up to the $S/B = 40\%$. The cell by virtue of its three dimensional nature, offers all round confinement to the encapsulated soil. The interconnected cells form a slab that behaves like a large pad that spreads the applied load over a wider area and hence improves the performance of the sand bed. The maximum bearing pressure was observed when the bed was reinforced with the combination of geocell and geogrid. The planar geogrid contributes in improving the overall performance of the bed by resisting the downward movement of soil due to the loading by virtue of membrane mechanism (Hegde and Sitharam, 2013). Hence, it is always beneficial to use the planar geogrid layer at the base of the geocell mattress.

Fig. 7 shows the variation of the vertical pressure on the top of the pipe for different reinforcement condition. For convenience, the measured pressure value (P_u) was normalized with maximum applied pressure (q_u). The reported pressure values are corresponding to the q_u value equal to the ultimate bearing pressure of the unreinforced bed (i.e.152 kPa). In the present case, the pressure values (P_u/q_u) observed in the unreinforced case was about 0.20. Similarly, the pressure values for different type of reinforcements were varied between 0.16 and 0.07. As compared to unreinforced bed, about 65% reduction in the pressure value was observed at the top of the pipe when the combination of geocell and geogrid was used.

Similarly, Fig. 8 represents the measured strain values on the top of the pipe. The reported strain values are compressive in nature and measured at the center of the pipe, exactly below the loading plate. Brachman et al. (2008) observed that the measured vertical strain value in a pipe wall could vary a great deal, depending on the point on the periphery at which strain is measured. Another important factor which influences the accumulation of the strain is stiffness of the pipe. Stiffer the pipe lesser is the accumulated strain. In the present case, the strain value observed in unreinforced case

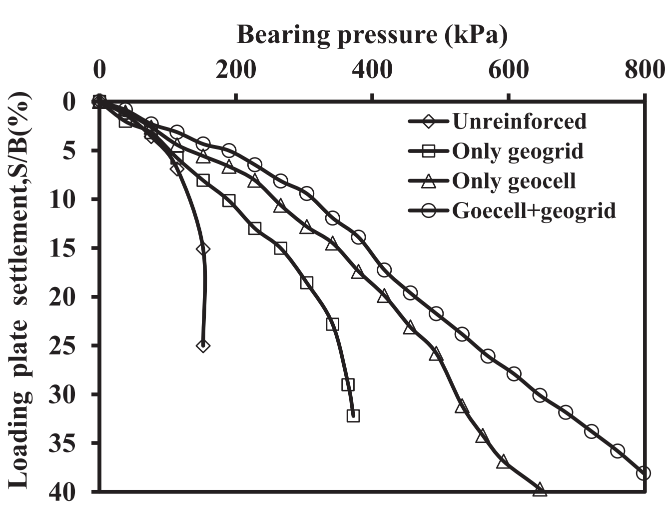

Fig. 6. Variation of bearing pressure with plate settlement for different type of reinforcements.

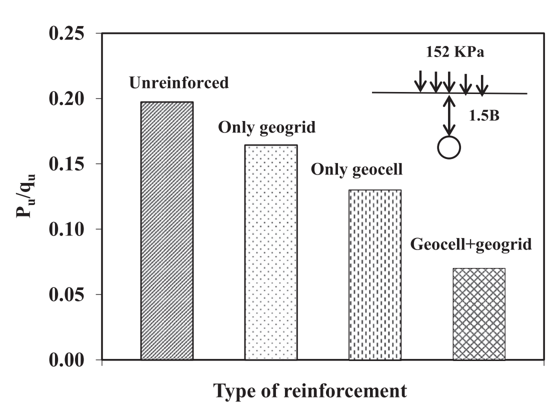

Fig. 7. Vertical pressure values at the top of the pipe for different type of reinforcement.

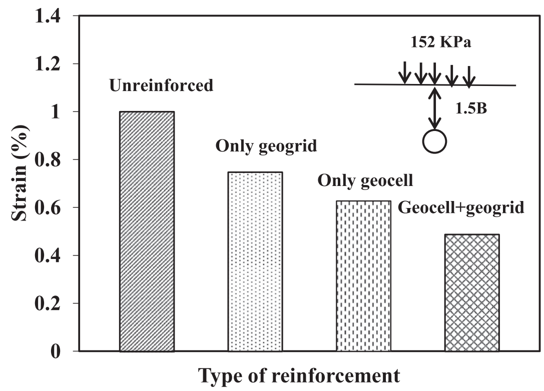

Fig. 8. Strain values at the top of the pipe for different type of reinforcement.

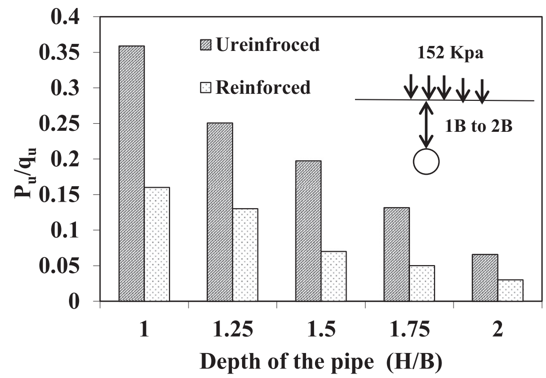

Fig. 10. Vertical pressure values at the top of the pipe for different depth of placement.

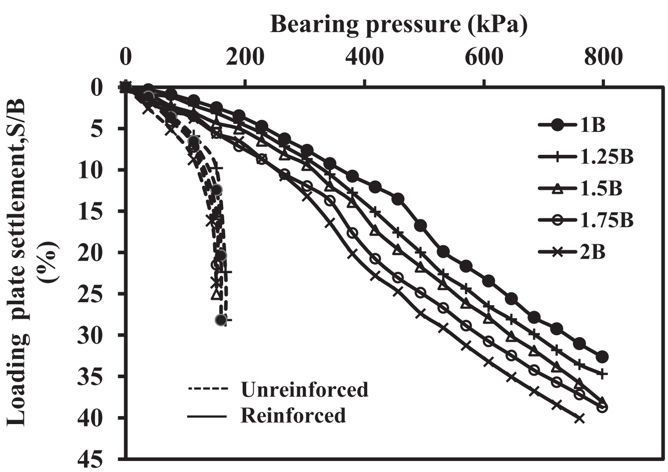

Fig. 9. Variation of bearing pressure with plate settlement for different depth of placement of pipe.

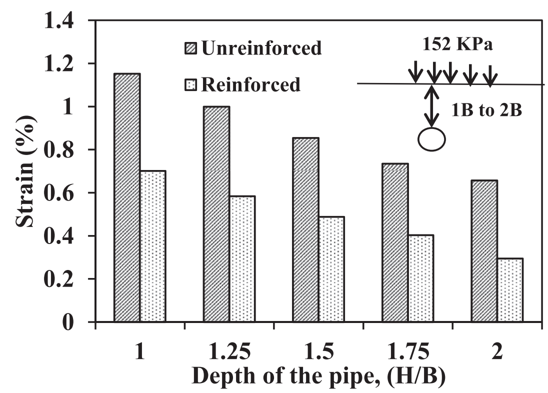

Fig. 11. Strain values at the top of the pipe for different depth of placement of pipe.

was about 0.85%. The strain values were varied between 0.74% and 0.48% for different forms of reinforcements. Similar strain values were reported by Tavakoli et al. (2012) in their studies. The least strain on the pipe was observed when the geocell with additional basal geogrid was used as the reinforcement. Compared to unreinforced case, 43% reduction in the strain was observed when the combination of geocell and geogrid was used. It should be noted that the reported strain values were corresponding to pipe depth of 1.5*B* and applied pressure value of 152 kPa, which is nothing but the ultimate bearing capacity of the unreinforced bed.

3.2. Effect of depth of placement of pipe

The geocell with additional basal geogrid found to provide better protection to buried pipelines as compared to other type of reinforcements. Hence, in this section the depth of placement of the pipe was varied between 1*B*–2*B* below the loading plate in the presence of geocell and geogrid reinforcement. The aim of the depth variation was to understand and compare the pressure and strain values experienced by the pipe at different depths. Fig. 9 represents the variation of bearing pressure with plate settlement at different depth of placement of the pipe. The performance of the sand bed was found to be marginally influenced by the position of the pipe, even in the presence of relatively stiff reinforcement system. As the depth of the pipe increase, the settlement increases and the bearing pressure decreases in all the cases. As the pipe stiffness is 2–3 times higher than the reinforcement system, the pipe itself acts as reinforcement along with the geocells.

Fig. 10 and Fig. 11 represent the measured pressure and strain values on the pipe at different depth of placement. The reported pressure and strain values are corresponding to the applied pressure value of 152 kPa, which is nothing but the ultimate bearing capacity of the unreinforced bed. The measured pressure values (P_u/q_u) found to vary between 0.35 and 0.06 for different depths for the unreinforced case. For the same depths, the P_u/q_u values found to vary between 0.16 and 0.003 for the reinforced case. More than 50% reduction in the pressure was observed in the presence of reinforcement as compared to the unreinforced case at all the depths. In the presence of reinforcement, at a depth below 1.5 *B*, the pressure value on the pipe reduced below 0.10, which is almost negligible. Similarly, the strain value found to vary between 1.15% and 0.65% for different depths for the unreinforced case. For the same depths, the strain values found to vary between 0.7% and 0.29% for the reinforced case. More than 40% reduction in the strain value was observed in the presence of reinforcement as compared to the unreinforced case at all the depths. The observed pressure and strain values indicate that the provision of the geocell with additional basal geogrid significantly reduces the depth of placement of the pipe. In the broader perspective, these findings will have huge implications in reducing the installation costs of the buried pipelines in large projects, where pipelines are laid along several hundreds of kilometers.

4. Numerical modeling

Numerical modeling was carried out using FLAC^{3D} considering its ability to model a wide range of geotechnical problems. FLAC^{3D} uses an explicit finite difference solution scheme to solve the initial and boundary value problems. It has several built-in material models and structural elements to model the variety of geomaterials and the reinforcements. It provides the option to use the interface elements to accurately model the joints and the interfaces between two materials. The simulation was carried out for unreinforced case and the geocell with additional basal geogrid reinforced case, when the pipe was placed at a depth of 1.5B below the loading plate. The dimension of the model was kept same as that of the dimension of test bed used in the experiments. The elastic-perfectly plastic Mohr Coulomb model was used to simulate the behavior of the subgrade soil and the infill soil. The geocell was modeled using the geogrid structural element while the pipe was modeled using the shell structural element available in FLAC^{3D}. Linear elastic model was used to simulate the behavior of the geocell and the pipe. The rigid nature of the geocell joint was simulated by fixing the nodes representing the joints. The interface between the geocell and the soil was linearly modeled with Mohr Coulomb yield criterion. Fig. 12 shows the skeleton view of the FLAC^{3D} model for the unreinforced and reinforced cases.

Analyses were carried out under controlled velocity loading of $2.5 \times E{-}5$ m/step. Only quarter portion of the test bed was modeled making use of the symmetry to reduce the computational effort. The quarter symmetric model of size 0.45 m × 0.45 m × 0.6 m was discretized into 10,320 zones. Sensitivity analyses were carried out to determine the mesh density and based on which, the relatively coarse mesh was chosen for the analysis. Preliminary analyses carried out revealed that the boundary distances did not influence the results as deformations and stresses were contained within the boundaries. The displacement along the bottom boundary (which represents tank bottom) was restrained in both horizontal as well as vertical directions. The side boundaries (which represent tank side) were restrained only in the horizontal direction, such that the displacements were allowed to occur in the vertical direction.

Table 3 represents properties of different materials used in the numerical simulations. Shear strength properties (C and φ) of the sand were determined from the direct shear test. The dilation angle was taken as 2/3rd of the friction angle as suggested by the earlier researchers in the similar studies in FLAC (Ghazavi and Lavasan, 2008; Madhavi Latha and Somwanshi, 2009). The elastic modulus (initial tangent modulus) of the sand was determined from the consolidated undrained triaxial compression test. The test was carried out at three different confining pressures of 100 kPa, 200 kPa and 300 kPa. Initial tangent modulus was determined from the stress-strain curve corresponding to the confining pressure of 200 kPa. From the elastic modulus, the shear modulus and the bulk modulus values were determined by assuming the Poisson's ratio of 0.3. The elastic modulus of the geocell, geogrid and the pipe was determined from tensile stress-strain curve shown in Fig. 3. The secant modulus corresponding to 2% axial strain was considered while calculating the modulus. Similarly, the Poison's ratio values provided by the manufacturer were used. The interface shear strength properties (c_i and φ_i) for both geocells and geogrid were obtained from the modified direct shear tests. In case of the geocells, the reported interface properties are corresponding to the interface between the sand and the geocell wall. In the modified direct shear test, the reinforcement was glued to a wooden plate and was placed in the lower half of the shear box such that the top surface of the reinforcement was along the horizontal shear plane

Table 3
Properties of different materials used in numerical modeling.

Parameters	Values
Sand	
Shear modulus, G (MPa)	5.77
Bulk modulus, K (MPa)	12.5
Poisson's ratio, μ	0.3
Cohesion, C (kPa)	0
Friction angle, φ (°)	36
Dilation angle, Ψ(°)	24
Unit weight, γ (kN/m^3)	20
Geocell	
Young's modulus, E (MPa)	275
Poisson's ratio, μ	0.45
Interface shear modulus, k_i (MPa/m)	2.36
Interface cohesion, c_i (kPa)	0
Interface friction angle, φ_i (°)	30
Thickness, t_i (mm)	1.5
Basal Geogrid	
Young's modulus, E (MPa)	210
Poisson's ratio, μ	0.33
Interface shear modulus, k_i (MPa/m)	2.36
Interface cohesion, c_i (kPa)	0
Interface friction angle, φ_i (°)	18
Thickness, t_i (mm)	1.5
Pipe	
Young's modulus, E (GPa)	3.1
Poisson's ratio, μ	0.4
Thickness, t_i (mm)	1.4

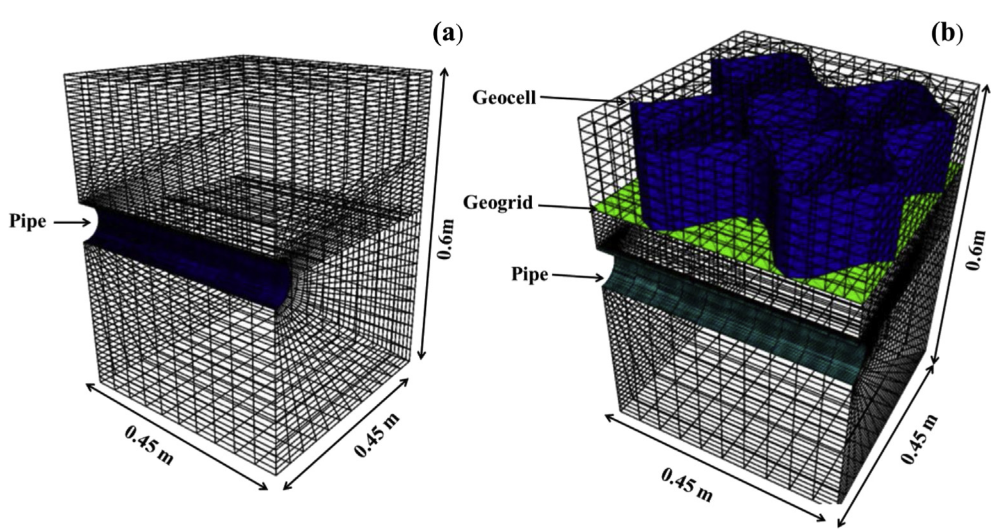

Fig. 12. Skeleton view of the FLAC^{3D} model: (a) unreinforced case; (b) geocell and geogrid reinforced case.

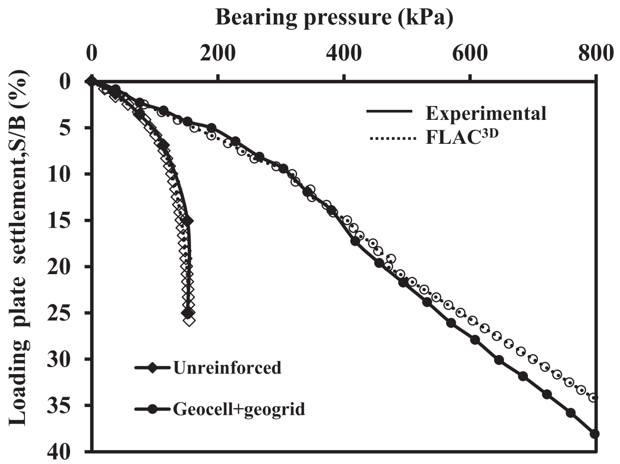

Fig. 13. Comparison of experimental and numerical bearing pressure-settlement curve.

(Srinivasa Murthy et al., 1993). The interface shear modulus value (k_i) of 2.36 MPa/m was considered in the analysis for geocells and geogrids (Itaska, 2008).

Fig.13 represents the comparison of the experimental and numerical bearing pressure-settlement curves for unreinforced and geocell with additional basal geogrid reinforced case, when the pipe was placed at a depth 1.5*B* below the loading plate. A good agreement in the results was obtained between the experimental and numerical studies. Numerical studies also revealed that the no failure of the sand bed, even up to large settlements in the presence of geocells. Fig. 14 shows the vertical stress distribution contours for unreinforced and the reinforced cases. These contours are corresponding to the settlement of $S/B = 33\%$. The tank boundaries found to have no influence on the results as the measured stresses adjacent to the boundary were equal to zero. A substantial reduction in the pressure transferred to the pipe was observed in the presence of the reinforcements. In case of the unreinforced soil, stress was found to distribute to a greater depth in the form of a narrow band. However, in case of geocells, the stress was found to distribute in the lateral direction to a shallow depth. Similar observations were also made by Saride et al. (2009) and Hegde and Sitharam (2015a, b) during the numerical simulations of the geocell reinforced soil beds. Since, geocell distribute the load in the lateral direction, the intensity of the stress will reduce on the soil existing blow the geocells. Therefore, the pipe will also experience the less stress in the presence of reinforcement as compared to the unreinforced beds.

Fig.15 shows the distribution of the vertical displacement contours on the surface of the pipe for unreinforced and the reinforced cases. The reported displacements are acting in the downward direction. From the figure it is evident that the deformation of the pipe significantly reduces in the presence of the geocells and geogrids. From the maximum value of the observed deformation, the strain on the pipe was deduced for both unreinforced and reinforced cases. The strain values thus calculated were 0.93% and 0.58% respectively for unreinforced and reinforced cases. As compared to experimentally obtained strain, the numerically obtained strain values were found to be 8%–9% higher for both the cases. This difference may be due of the material properties used in the numerical simulations.

5. Scale effects

Though full scale model tests are the most reliable means of studying the behavior of the prototypes, at times these tests become cumbersome. In those cases, reduced scale model tests are performed at 1-g condition. 1-g model tests help to obtain the approximate information about the general behavior of the prototypes quicker than the full scale testing with closer control over the key parameters. However, the results of 1-g model tests are prone to scale effects. Hence, the results obtained from the 1-g model tests are not directly applicable to the prototype case.

As suggested by Fakher and Jones (1996), the results of the small scale model tests can be extrapolated to prototype cases by carefully applying the scaling laws. Dimensional analysis can be used to deduce the scaling laws involving the relationship between the parameters that could affect the phenomenon that is being modeled. The theory of dimensional analysis is explained in detail elsewhere by Buckingham (1914). Generally, the dimensions of the variables are expressed in the combinations of three fundamental units, namely, length (L), mass (M) and time (T). However, Butterfield (1999) highlighted that application of dimensional analysis can produce misleading results in some cases, unless the alternative grouping for force $[MLT^{-2} = F]$ is used as a member of the fundamental system. Hence, in most of the geotechnical

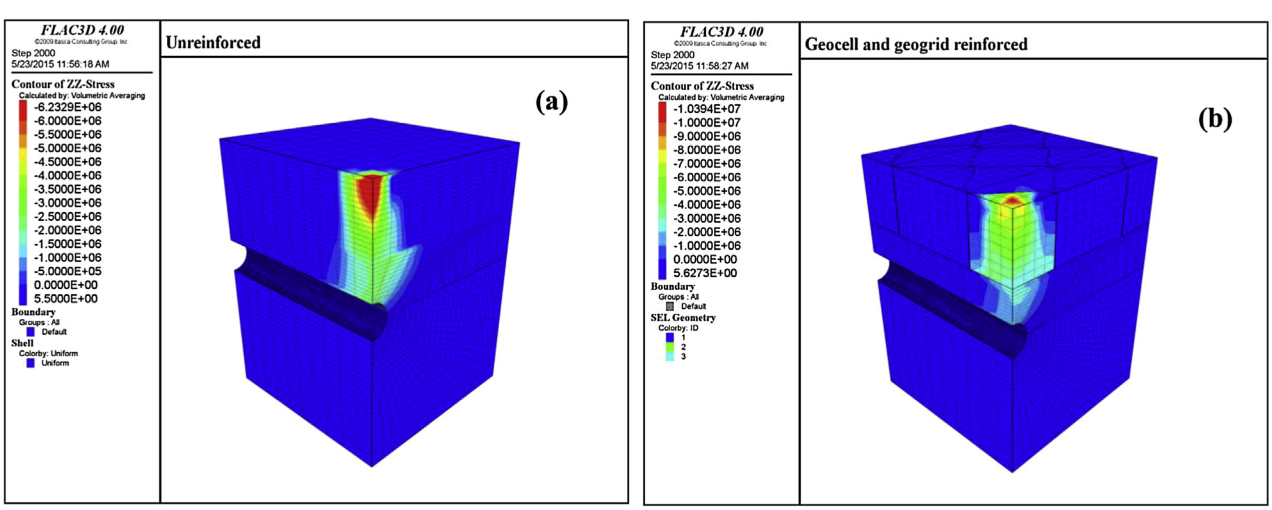

Fig. 14. Vertical stress distribution (N/m^2): (a) unreinforced case; (b) geocell and geogrid reinforced case.

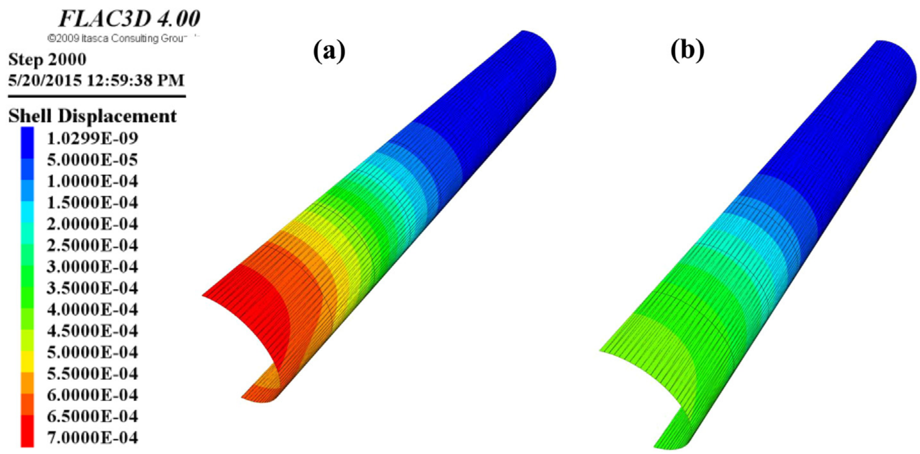

Fig. 15. Deformation on the pipe (m): (a) unreinforced case; (b) geocell and geogrid reinforced case.

problems force (F) and length (L) are used as the two fundamental dimensions.

In the present case, the major influencing parameters are, B, D, H, h, d, b, u, S, K_g, K_p, G, γ, φ, q_r,q_u. where K_g and K_p are the stiffness of the geocell and the pipe, respectively; G is the shear modulus of the sand; S is the settlement of the loading plate; γ is the unit weight of the sand; φ is the friction angle of the sand; q_r and q_u are the ultimate bearing capacity of the reinforced and unreinforced case respectively. Please refer Fig. 5 for the description of remaining geometric properties used in the study.

The function (f) that governs the present system can be represented as,

$$f(B, D, H, h, d, b, u, S, Kg, Kp, G, \gamma, \phi, qr, qs) = 0 \quad (1)$$

There are 15 influencing parameters present in Eq. (1) and the model involves only two fundamental dimensions i.e. force (F) and length (L). Hence, the present system might be studied by a complete set of 13 independent dimensionless parameters as described below.

$$g(\pi_1, \pi_2, \pi_3, \pi_4 ....\pi_{13}) = g\left[\left(\frac{D}{B}\right), \left(\frac{H}{B}\right), \left(\frac{h}{B}\right), \left(\frac{d}{h}\right), \left(\frac{d}{B}\right), \left(\frac{b}{B}\right), \left(\frac{u}{B}\right), \left(\frac{S}{B}\right), \left(\frac{K_g\gamma}{G^2}\right), \left(\frac{K_p\gamma}{G^2}\right), \left(\frac{G}{\gamma B}\right), \left(\frac{q_s}{q_u}\right), \phi, \right] = 0 \quad (2)$$

where g is the function that governs the system. The π terms (π_1 to π_{13}) reported in Eq. (2), should be same for model and prototype. Considering the width of the prototype plate will be N times higher than the model plate,

$$\frac{B_p}{B_m} = N \quad (3)$$

where N is the scaling factor; subscripts p and m refer to prototype and model respectively. Equating, $(\pi_{11})_p = (\pi_{11})_m$

$$\left(\frac{G}{\gamma B}\right)_p = \left(\frac{G}{\gamma B}\right)_m \quad (4)$$

It is very important to maintain the soil properties same in both model and prototype in order to avoid the particle size effect. Hence, the unit weight of the soil (γ) must be same in model and prototype. Eq. (4) can be re-written as,

$$\left(\frac{G_p}{G_m}\right) = \left(\frac{B_p}{B_m}\right) = N \quad (5)$$

Similarly, equating, $(\pi_9)_p = (\pi_9)_m$

$$\left(\frac{K_g\gamma}{G^2}\right)_p = \left(\frac{K_g\gamma}{G^2}\right)_m \quad (6)$$

Rewriting the Eq. (6),

$$\left(\frac{K_{g(p)}}{K_{g(m)}}\right) = \left(\frac{G^2{}_p}{G^2{}_m}\right) = N^2 \quad (7)$$

As per Eq. (7) the stiffness of the reinforcement to be used in the prototype should be N^2 times the stiffness of the reinforcement used in the model. Sireesh et al. (2009) observed that the stiffness of the geocell joint that decides the performance of the geocell than the stiffness of the material from which it is made. In the same line, it is possible to obtain the stiffness of the pipe to be used in the prototype as N^2 times the stiffness of the pipe used in the model.

Based on the scaling law deduced above, the results are extrapolated to the prototypical case of the shallow pipeline below the pavement. Generally, the diameter of the tire contact is about 0.3 m. The steel plate width used in the present study is 0.15 m. Hence, the scale factor can be deduced as,

$$\frac{B_p}{B_m} = \frac{0.3}{0.15} = 2 = N \quad (8)$$

The ultimate tensile strength of the prototype reinforcement should be 80 kN/m (20 kN/m × 4). Generally, bamboo will have the ultimate tensile strength in that range. 3-dimensional cells prepared from the bamboo strips known as bamboo cells could be used in the prototype pavement applications. The beneficial aspects of the bamboo cells and other details are explained elsewhere by

Hegde and Sitharam (2014c). Similarly, the diameter and the thickness of the prototype pipe turns out to be 0.15 m (2 × 0.075) and 2.8 mm (1.4 mm × 2) respectively. The ultimate tensile strength of the prototype pipe should be 168 kN/m (42 kN/m × 4). Generally cast iron pipes will have the tensile strength in that range. Fakher and Jones (1996) warned that, it is not feasible to use complete similarity between model and prototype due to involvement of several complex factors. It should be left to the judgment of the researchers to decide about the factors to scale up considering the accuracy and the nature of the problem. In the present study, the scaling laws suggested using the geocell of bigger pocket size i.e. 0.5 m in the prototype applications. However, it is recommended to use the geocells of smaller pocket size in the prototype applications similar to the model studies.

6. Conclusions

Experimental studies have been conducted to explore the possibility of using the geocells in protecting the underground utilities and buried pipelines. Results suggest that the use of geocells with additional basal geogrid significantly reduces the deformation of the pipe as compared to other type of reinforcements used in the study. Further, the depth of the placement of the pipe was varied between 1*B* to 2*B* below the loading plate in the presence of geocells and geogrids. The measured pressure/strain values in the reinforced case were compared with the pressure/strain values measured at the same depth for the unreinforced case. More than 50% reduction in the pressure and more than 40% reduction in the strain values were observed in the presence of reinforcement at all the depths. The pressure on the pipe becomes almost negligible (i.e, $P_u/q_u < 0.1$) beyond the depth of 1.5*B* below the loading plate in the presence of geocells. The observed pressure and strain values indicate that the provision of the geocells significantly reduces the depth of placement of the pipe. In a broader perspective, these findings will help to reduce the installation costs of the buried pipelines in large projects, where pipelines are laid along several hundreds of kilometers. Further, numerical simulations were carried out using FLAC^{3D} to understand the distribution of the stresses and strains in the pipe. Modeling results revealed that the geocells distribute the load in the lateral direction to a shallow depth, thus reducing the pressure on the pipe. A good agreement in measured stain values on the pipe was observed between the experimental and numerical studies.

The study has some limitations. Only one type backfill soil and only one type of pipe were used in the study. Hence, it should be noted that the results are applicable to the limited cases. Further studies are necessary with different types of the pipe, soil, and the loading conditions. It should be noted that the observed results may vary significantly for the pipes with different stiffness values.

Acknowledgment

The first author is thankful to Mr. Sharan Kadabinakatti (graduate research student) for his help in carrying out the laboratory model tests in the initial stage of this study.

List of notations

b	width of the geocell mattress(m)
B	width of the steel plate (m)
C	cohesion (kPa)
C_c	coefficient of curvature (dimensionless)
c_i	interface cohesion (kPa)
C_u	coefficient of uniformity (dimensionless)
d	pocket size of geocell (m)
D	diameter of the pipe (m)
D_{10}	effective particle size (mm)
e_{max}	maximum void ratio of sand (dimensionless)
e_{min}	minimum void ratio sand (dimensionless)
G	shear modulus of sand (MPa)
γ	unit weight of sand (kN/m^3)
h	height of the geocell mattress (m)
H	depth of placement of pipe (m)
k_i	interface shear modulus (MPa/m)
K_g	stiffness of the geocell (kN/m)
K_p	stiffness of the pipe (kN/m)
L	length in general (m)
M	mass in general (kg)
N	scale factor (dimensionless)
T	time in general (sec)
F	force in general (N)
P_u	measured stresses on top of the pipe (kPa)
q_u	applied pressure at the top of the bed (kPa)
q_r	ultimate bearing capacity of the reinforced bed (kPa)
q_s	ultimate bearing capacity of the unreinforced bed (kPa)
S	settlement of the loading plate (mm)
u	depth of placement of the geocell(m)
φ	friction angle of the sand (degrees)
φ_i	interface friction angle between geocell and sand (degrees)

References

Almeida, M., Hosseinpour, I., Riccio, M., Alexiew, D., 2014. Behavior of geotextile encased granular columns supporting test embankment on soft deposit. J. Geotech. Geoenvironmental Eng. http://dx.doi.org/10.1061/(ASCE)GT, 1943-5606.0001256, 04014116.
Arockiasamy, M., Chaallal, O., Limpeteeparakarn, T., 2006. Full-scale field tests on flexible pipes under live load application. J. Perform. Constr. Facil. 20 (1), 21–27.
ASTM D4885, 2011. Standard Test Method for Determining Performance Strength of Geomembranes by Wide Strip Tensile Method. ASTM International, West Conshohocken, PA, USA.
ASTM D638, 2010. Standard Test Method for Tensile Properties of Plastics. ASTM International, West Conshohocken, PA, USA.
ASTM D6637, 2011. Standard test method for determining the tensile properties of geogrid by the single or multi-rib tensile method. ASTM International, West Conshohocken, PA, USA.
Bai, Xiao-Hong, Huang, Xian-Zhi, Zhang, Wei, 2013. Bearing capacity of square footing supported by a geobelt-reinforced crushed stone cushion on soft soil. Geotext. Geomembr. 38, 37–42.
Brachman, R.W.I., Moor, I.D., Rowe, R.K., 2000. The design of a laboratory facility for evaluating the structural response of small diameter buried pipe. Can. Geotech. J. 37 (2), 281–295.
Brachman, R.W.I., Moore, I.D., Munro, S.M., 2008. Compaction effects on strains within profiled thermoplastic pipes. Geosynth. Int. 15 (2), 72–85.
Buckingham, E., 1914. On physically similar systems; illustrations of the use of dimensional equations. Phys. Rev. 4 (4), 345–376.
Butterfield, R., 1999. Dimensional analysis for geotechnical engineers. Geotechnique 49 (3), 357–366.
Dash, S.K., Krishnaswamy, N.R., Rajagopal, K., 2001. Bearing capacity of strip footings supported on geocell reinforced sand. Geotext. Geomembr. 19, 235–256.
Demir, Ahmet, Laman, Mustafa, Yildiz, Abdulazim, Ornek, Murat, 2013. Large scale field tests on geogrid reinforced granular fill underlain by soft clay. Geotext. Geomembr. 38, 1–15.
Fakher, A., Jones, C.J.F.P., 1996. Discussion on bearing capacity of rectangular footings on geogrid reinforced sand. by Yetimoglu, T., Wu, J.T.H., Saglamer, A., 1994 J. Geotech. Eng. 122, 326–327.
Ghazavi, M., Lavasan, A.A., 2008. Interference effect of shallow foundations constructed on sand reinforced with geosynthetics. Geotext. Geomembr. 26 (5), 404–415.
Hegde, A., Sitharam, T.G., 2013. Experimental and numerical studies on footings supported on geocell reinforced sand and clay beds. Int. J. Geotech. Eng. 7 (4), 347–354.
Hegde, A., Sitharam, T.G., 2014a. Joint strength and wall deformation characteristics of a single cell subjected to uniaxial compression. Int. J. Geomech. http://dx.doi.org/10.1061/(ASCE)GM, 1943-5622.0000433.
Hegde, A.M., Sitharam, T.G., 2014b. Effect of infill materials on the performance of geocell reinforced soft clay beds. Geomech. Geoengin. http://dx.doi.org/10.1080/17486025.2014.921334.
Hegde, A., Sitharam, T.G., 2014c. Use of bamboo in soft ground engineering and its performance comparison with geosynthetics: experimental studies. Mater. Civ. Eng. http://dx.doi.org/10.1061/(ASCE)MT, 1943-5533.0001224.

Hegde, A., Sitharam, T.G., 2015a. 3-dimensional numerical modeling geocell reinforced sand beds. Geotext. Geomembr. http://dx.doi.org/10.1016/j.geotexmem.2014.11.009.
Hegde, A.M., Sitharam, T.G., 2015b. 3-Dimensional numerical analysis of geocell reinforced soft clay beds by considering the actual geometry of geocell pockets. Can. Geotech. J. http://dx.doi.org/10.1139/cgj-2014-0387.
Hegde, A., Kadabinakatti, S., Sitharam, T.G., 2014. Protection of Buried Pipelines Using a Combination of Geocell and Geogrid Reinforcement: Experimental Studies. Ground Improvement and Geosynthetics, Geotechnical Special Publication-238, ASCE, pp. 289–298.
Indraratna, B., Nimbalkar, S., Christie, D., Rujikiatkamjorn, C., Vinod, J., 2010. Field assessment of the performance of a ballasted rail track with and without geosynthetics. Geotech. Geoenvironmental Eng. 136, 907–917.
Indraratna, B., Biabani, M., Nimbalkar, S., 2014. Behavior of geocell reinforced subballast subjected to cyclic loading in plane strain condition. J. Geotech. Geoenvironmental Eng. http://dx.doi.org/10.1061/(ASCE)GT, 1943-5606.0001199.
Itaska, 2008. Fast Lagrangian Analysis of Continua (FLAC3D 4.00). Itasca Consulting Group Inc, Minneapolis, USA.
Lambert, S., Nicot, F., Gotteland, P., 2011. Uniaxial compressive behavior of scrapped tire and sand filled wire netted geocell with a geotextile envelop. Geotext. Geomembr. 29, 483–490.
Madhavi Latha, G., Somwanshi, A., 2009. Effect of reinforcement form on the bearing capacity of square footing on sand. Geotext. Geomembr. 27, 409–422.
Mehdipour, Iman, Ghazavi, Mahmoud, Moayed, R.Z., 2013. Numerical study on stability analysis of geocell reinforced slopes by considering the bending effect. Geotext. Geomembr. 37, 23–34.
Tavakoli Mehrjardi, Gh, Moghaddas Tafreshi, S.N., Dawson, A.R., 2012. Combined use of geocell reinforcement and rubber soil mixtures to improve performance of buried pipes. Geotext. Geomembr. 34, 116–130.
Tavakoli Mehrjardi, Gh, Moghaddas Tafreshi, S.N., Dawson, A.R., 2013. Pipe response in a geocell-reinforced trench and compaction considerations. Geosynth. Int. 20 (2), 105–118.
Mir Mohammad Hosseini, S.M., Moghaddas Tafreshi, S.N., 2002. Soil structure interaction of embedded pipes under cyclic loading conditions. Int. J. Eng. 15 (2), 117–124.
Moghaddas Tafreshi, S.N., Dawson, A.R., 2010. Behavior of footings on reinforced sand subjected to repeated loading comparing use of 3D and planar geotextile. Geotext. Geomembr. 28, 434–447.
Moghaddas Tafreshi, S.N., Khalaj, O., 2008. Laboratory tests of small-diameter HDPE pipes buriedin reinforced sand under repeated-load. Geotext. Geomembr. 26, 145–163.
Moghaddas Tafreshi, S.N., Khalaj, O., Dawson, A.R., 2014. Repeated loading of soil containing granulated rubber and multiple geocell layers. Geotext. Geomembr. 42, 25–38.
Srinivasa Murthy, B.R., Sridharan, A., Bindumadhava, 1993. Evaluation of interfacial frictional resistance. Geotext. Geomembr. 12, 235–253.
Palmeira, E.M., Andrade, H.K.P.A., 2010. Protection of buried pipes against accidental damage using geosynthetics. Geosynth. Int. 17 (4), 228–241.
Pokharel, S.K., Han, J., Leshchinsky, D., Parsons, R.L., Halahmi, I., 2010. Investigation of factors influencing behavior of single geocell reinforced bases under static loading. Geotext. Geomembr. 28 (6), 570–578.
Rowe, R.K., Taechakumthorn, C., 2011. Design of reinforced embankments on soft clay deposits considering the viscosity of both foundation and reinforcement. Geotext. Geomembr. 29, 448–461.
Saride, S., Gowrisetti, S., Sitharam, T.G., Puppala, A.J., 2009. Numerical simulations of sand and clay. Ground Improv. 162 (GI4), 185–198.
Sireesh, S., Sitharam, T.G., Dash, S.K., 2009. Bearing capacity of circular footing on geocell sand mattress overlying clay bed with void. Geotext. Geomembr. 27 (2), 89–98.
Sitharam, T.G., Hegde, A., 2013. Design and construction of geocell foundation to support the embankment on settled red mud. Geotext. Geomembr. 41, 55–63.
Srivastava, A., Goyal, C.R., Raghuvanshi, A., 2012. Load settlement response of footing placed over buried flexible pipe through a model plate load test. Int. J. Geomech. 13 (4), 477–481.
Thakur, J.K., Han, Jie, Pokharel, S.K., Parsons, R.L., 2012. Performance of geocell-reinforced recycled asphalt pavement (RAP) bases over weak subgrade under cyclic plate loading. Geotext. Geomembr. 35, 14–24.
Yang, X., Han, J., Pokharel, S.K., Manandhar, C., Parsons, R.L., Leshchinsky, D., Halahmi, I., 2012. Accelerated pavement testing of unpaved roads with geocell reinforced sand bases. Geotext. Geomembr. 32, 95–103.